

Magneto-thermoelectric current induced by phonon drag in low-dimensional junctions

S. E. Shafranjuk

Department of Physics and Astronomy, Northwestern University, Evanston, IL 60208

(Dated: February 27, 2018)

We examine splitting the heat flow in a low-dimensional junction under influence an external d.c. magnetic field. The junction is a crossing between the narrow single atomic layer stripe (or a nanotube) of a semiconductor C with a metal stripe N (C/N-knot). External source of heat injects the non-equilibrium (NE) phonons, electrons, and holes into C which then propagate in direction the C/N-knot. Most of the heat is carried by NE phonons which drag additional electron and hole excitations along C. In vicinity the C/N-knot, the Lorentz force pulls the charge carriers from C to N thus inducing a substantial lateral magneto-thermoelectric electric current (MTEC) along N.

PACS numbers: 84.60.Rb, 73.40.Gk, 73.63.Kv, 44.20.+b

Magneto-thermoelectric phenomena attract significant attention of many researchers because they provide fundamental knowledge about transport the charge carriers and phonons in low-dimensional conductors. [1, 2] Thermoelectricity also finds a variety of applications in scientific research and engineering. Controlling the heat flow by an external field is important, e.g., in processes of thermoelectric cooling and energy generation. [3–7] On this path, novel single atomic layer materials have a great potential. [4–7]

In this Letter we show that the heat stream along a narrow single atomic layer semiconducting stripe or nanotube C causes magneto-thermoelectric current (MTEC) arising in a narrow metal stripe N which is crossing C in perpendicular direction. The MTEC arises from splitting

the heat flow under influence an external d.c. magnetic field $\mathbf{B} = \{0, 0, B_z\}$ which is applied to the C/N crossing (we call it the C/N-knot which is sketched in Fig. 1). The heat flow emerges by injecting of non-equilibrium (NE) excitations from the external heater H into the C'' section of C as shown in Fig. 1a. The effective local temperature T^* in C'' is considerably higher than the equilibrium temperature T_C of the C ends. The NE injection causes a finite thermal current $Q = \Lambda (T^* - T_C)$ along C where the heat conductance $\Lambda = \Lambda_{ph} + \Lambda_e + \Lambda_h$ consists of the phonon (Λ_{ph}), electron (Λ_e), and hole (Λ_h) components. [8, 9] If number the NE electrons and holes which are excited in C is equal to each other (like, e.g., in undoped graphene or carbon nanotubes), the electric charge transferred along C is zero, i.e., $I_{||} \equiv 0$. Another scenario might take place if the effective electron temperature T^* is lower than the exciton binding energy E_g whereas the NE charge carrier density n^* is high. Then the electrons and holes could form the excitons which are also contributing to the heat transfer in C. In this Letter, however, we mostly consider the case $T^* > E_g$. Because in C (likewise in carbon nanotubes or in graphene) $\Lambda_{ph} \gg \max\{\Lambda_e, \Lambda_h\}$, most of the heat along C is carried by phonons. [8, 9] The phonons also drag additional electrons and holes along C at expense of the phonon-electron collisions. [10, 11]

Here we find that the Lorentz force acting in vicinity the C/N-knot splits the heat stream by pulling the electric charge carriers from C to N while the phonons are propagating further ahead. It results in a substantial electric current $I_{\perp} \neq 0$ which is formed in the lateral \hat{y} -direction along N, despite $I_{||} \equiv 0$. The non-equilibrium (NE) electron and hole excitations are created inside C by two mechanisms. (i) Phonon drag the electrons and holes along C, and (ii) Non-equilibrium thermal injection from the heat source H into C (see Fig. 1a). The heat flow splitting in the C/N-knot becomes possible due to the following. We assume that the C'/N-interface transparency $\mathcal{T}_{e,h}^{CN}$ for electrons and holes transmitted from C' to N is high ($\mathcal{T}_{e,h}^{CN} \lesssim 1$). Simultaneously, the same C'/N-interface transparency \mathcal{T}_{ph}^{CN} is very low for phonons

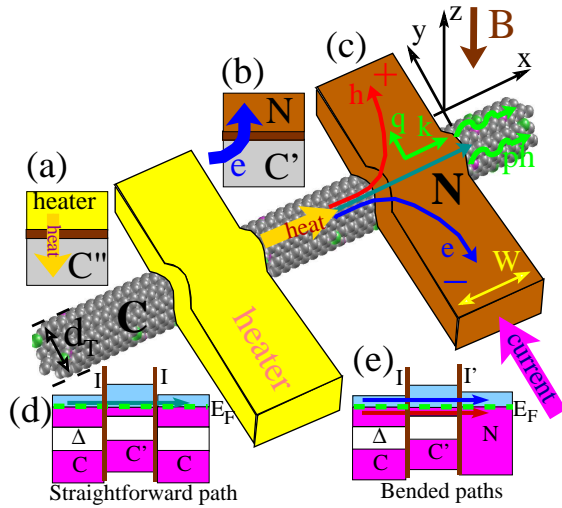


FIG. 1: Color online. (a) Heat injection into the C''-section under metal N. (b) Electron tunneling from the C'-section into the metal stripe N. (c) Main figure: Splitting the heat flow by the C/N-junction (C/N-knot in the nanotube-stripe cross geometry) when a finite d.c. magnetic field \mathbf{B} is applied in perpendicular to the knot's plane. (d) and (e) are two different energy diagrams which correspond to distinct electron trajectories C/C'/C and C/C'/N correspondingly.

(i.e., $\mathcal{T}_{ph}^{CN} \ll 1$) though their propagation inside C is ballistic. That happens because redirecting the phonons from C to N requires a significant change of the phonon's momentum $\Delta \mathbf{q} = \hat{\mathbf{y}}q_N - \hat{\mathbf{x}}q_C$ where q_N and q_C are the phonon momentum components along N and C respectively. [8, 9] Acoustic properties of C and N are very different as well: Not only they have distinct phonon spectra but the geometries of C and N might differ from each other. For instance, C could be a cylinder shaped nanotube whereas the metal stripe has a bar shape. Therefore for the sake of simplicity we disregard the phonon transmission from C to N by setting $\mathcal{T}_{ph} \simeq 0$. Thus we assume that phonons merely pass the knot and propagate along C further ahead. On the contrary, we will see that the Lorentz force easily redirects the non-interacting electrons and holes from C into the perpendicular metal stripe N. As it follows from further calculations, the redirection happens because the Lorentz force pulls electrons to the right (blue arrow in main Fig. 1c) whereas it pushes the holes to the left (red arrow in Fig. 1c). In this way, the heat flow (yellow arrow in Figs. 1a,c) along C induces the electric current I_{\perp} (magenta arrow) in N (brown).

We compute the electric current I_{\perp} induced in the C/N-knot under influence the d.c. magnetic field $\mathbf{B} = (0, 0, B_z)$. Let us assume that an electron which emerges from the left open C section then penetrates into the C' section under metal N (see Fig. 2a). At the next stage there are actually three further possible distinct trajectories for an electron to pass through the knot. (a) The electron is then transmitted into the right wing of N (blue arrow in Fig. 2a); (b) It can also proceed straightforward through the knot from C' to C on the opposite right hand side (green arrow in Fig. 2a); (c) Instead of being transmitted from C' to the right N-wing, an electron gets into the 'wrong' left N-wing (red arrow in the same figure). We emphasize that only the e^- and h^- -deflected trajectories (see correspondingly the blue and red lines in Fig. 1c) which energy diagram is shown in Fig. 1e contribute into the electric current generated along N. They correspond to an asymmetric C/C'/N-junction sketched in Fig. 1e. On the contrary, the straightforward trajectory shown by the green line in Fig. 1c and which is related to a symmetric C/C'/C junction (see energy diagram in Fig. 1d) gives no contribution into the electric current generated along N. The C/C' and C'/N interfaces might additionally contain potential barriers I originating from atomic impurities (shown as brown in Fig. 1a,b,d,e), imperfections, and/or difference the workfunctions of N and C. The lateral electric current generated in N is calculated using the Landauer-Büttiker formula

$$I_{\perp} = I_{\text{left}} - I_{\text{right}} = \frac{2e}{h} \int_0^{\infty} d\varepsilon M_{\min}(\varepsilon) \times 2 (\mathcal{T}_y^{\text{left}}(\varepsilon) - \mathcal{T}_y^{\text{right}}(\varepsilon)) (f_C(\varepsilon - \mu) - f_N(\varepsilon)) \quad (1)$$

where $M_{\min}(\varepsilon)$ is the minimum number of quantum

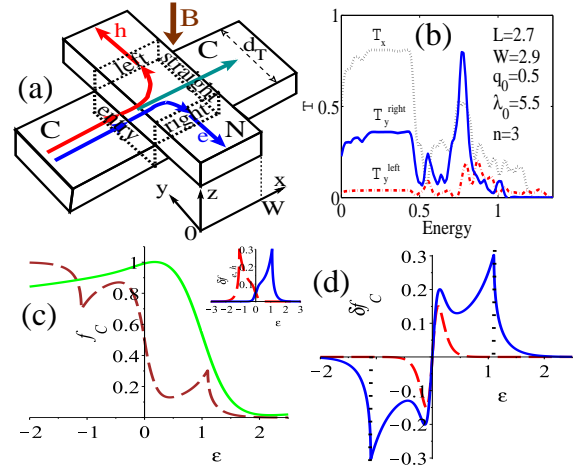


FIG. 2: Color online. (a) A cross-stripe geometry used in addition to the nanotube/stripe cross geometry shown in Fig. 1c for computing the transmission probabilities through the C/N-knot. (b) The transmission coefficients for an electron incoming from C into the C'-section along the \hat{x} -direction, T_x (dotted black curve), turning to the right, T_y^{right} (solid blue curve), and turning to the left, T_y^{left} (dashed red curve) computed for geometry (a) by solving non-linear boundary conditions. (c) The non-equilibrium (NE) electron distribution function $f_C(\varepsilon)$ in the C section. Brown curve is $f_C(\varepsilon)$ which is altered only by the NE phonon drag whereas green curve is $f_C(\varepsilon)$ altered only by thermal injection the electron and holes (see parameters in text). Inset shows the phonon drag-induced NE deviation the distribution function $\delta f_{e,h}$ of electrons (blue curve) and holes (red curve) in the C section for the same parameters. (d) Driving factor for the lateral magnetoelectric current at $U_0 = 0$. Red dashed curve corresponds to influence of the NE thermal injection only while blue solid curve shows the combined influence of both, the NE thermal injection and the phonon drag.

channels per energy interval, $\mathcal{T}_y^{\text{left(right)}}(\varepsilon)$ is the C/C'/N knot transparency for an electron to penetrate from section C through section C' into the left (or right) wing of N, $\mu \simeq U_0$ is the electrochemical potential shift inside C. A finite electric potential U_0 arises, e.g., due to coupling between the electron orbitals in N and C'. An extra factor 2 in Eq. (1) comes from the hole contribution into the lateral electric current I_{\perp} .

The lateral electric current I_{\perp} induced by the phonon drag and the thermal injection [12] depends on electron and phonon distribution functions f_C and N_C inside the C' section. The kinetic equations are

$$\dot{f}_C = \mathcal{L}_{th} + \mathcal{L}_{ep} \quad (2)$$

$$\dot{N}_C = \mathcal{P}_{th} + \mathcal{P}_{pe} \quad (3)$$

where \mathcal{L}_{th} and \mathcal{P}_{th} describe thermal injection of the non-equilibrium electrons, holes, and respectively phonons from the heat source H into the C'' section as shown in Fig. 1a, \mathcal{L}_{ep} is the electron-phonon collision integral, whereas \mathcal{P}_{pe} is the phonon-electron collision inte-

gral. In Eqs. (2), (3) we have disregarded other processes having a lesser importance. Phonon drag is essential in semiconducting nanotubes (stripes) whereas it is negligible in metallic nanotubes (stripes). The drag occurs [10, 25] when NE phonons with frequency Ω_0 propagating between the hot (C'') and cold (C') spots of the same C generate electrons and/or holes moving in the same direction during the phonon-electron collisions. In Eq. (1), the electron distribution functions $f_C = f_C^{(0)}(T_C'') + \delta f^{\text{th}} + \delta f^{\text{pd}}$ significantly deviates from its equilibrium value $f^{(0)}(T_C) = 1/(\exp(\varepsilon/T_C) + 1)$ due to the thermal injection from H to C'' by δf^{th} and due to the phonon drag generation by δf^{pd} . The NE deviations δf^{th} and δf^{pd} are computed using Eqs. (2), (3). The electron distribution function f_N taken in the left and right wings of the N-stripe $f_N^{\text{left/right}}$ do not much differ from each other (i.e., $f_N^{\text{left}} \simeq f_N^{\text{right}}$). Therefore we merely regard them as equilibrium by setting $f_N \simeq f^{(0)}(T_C')$ and characterize them by temperature T_C' . Besides we neglect by the jump of electric potential along N coming across the C/N-knot in the \hat{y} -direction. Eq. (2) with \mathcal{L}_{th} had been addressed in Ref. [12] whereas the phonon drag had been considered in Refs. [6, 10, 25]. On one hand, a small deviation δf^{pd} is obtained from Eq. (2) as

$$\delta f^{\text{pd}} \simeq \pi \tau_{ep} g^2 \sum_{i=\pm} |m(q_i)|^2 \delta N(sq_{\pm}) [f_i + f^{(0)} - 2f^{(0)} f_i] \quad (4)$$

where τ_{ep} is the electron-phonon collision time, $f^{(0)}(\varepsilon) = 1/(\exp(\varepsilon/T) + 1)$, $f_{\pm}(\varepsilon) = 1/\left(\exp\left(\sqrt{\varepsilon^2 + v^2 q_{\pm}^2} + 2q_{\pm} v \sqrt{\varepsilon^2 - v^2 q_{\pm}^2}/T\right) + 1\right)$, $q_{\pm} = 2\left(k \pm (s/v) \sqrt{k^2 + q_v^2}\right) / \left((s/v)^2 - 1\right)$, s is the speed of sound, and v is the Fermi velocity in C. On the other hand, the thermal injection changes f_C as

$$\delta f^{\text{th}} = \frac{\tau_{ep} \Gamma_{HC}}{1 + \tau_{ep} \Gamma_{HC}} (f_{C''} - f^{(0)}) \quad (5)$$

where Γ_{HC} is the electron tunneling rate between H and C, $f_{C''} = 1/(\exp(\varepsilon/T_{C''}) + 1)$. The NE deviation $\delta N = N_C - N^{(0)}$ from the Bose-Einstein function $N^{(0)}$ inside C entering (4) is found from Eq. (3) in the form

$$\delta N(\omega) = N_0 \exp\left(-(\omega - \Omega_0)^2 / \sigma_{ph}\right) \quad (6)$$

where the parameters N_0 , Ω_0 , and σ_{ph} are the amplitude, frequency, and width of the NE phonon beam propagating along C from C'' to C' . They are determined by boundary conditions, computed microscopically, and/or extracted from the experiment. Intensity N_0 the phonon beam (6) inside C is determined by power the heat source H, and by the H/C-interface transparency $\mathcal{T}_{ph}^{\text{HC}}$. The beam width σ_{ph} depends on the geometry of H.

Transmission probability through the C/N-knot is computed using two different geometries depicted in

Figs. 1c and 2a. As a trial wavefunction $\Psi_{C'}(x, y)$ for cross-stripe geometry in Fig. 2a we use a two-dimensional electron wave inside the rectangular box C' under the metal N. We assume that an electron with the \hat{x} -component momentum k enters the C/N-knot on the left side from C to C' at $x = 0$ and $0 < y < d_T$. The electron exits the C/N-knot to N either on right ($y = 0$, $0 < x < W$), on left ($y = d_T$, $0 < x < W$), or to C straight ($x = W$, $0 < y < d_T$) where W is the metal stripe width, and d_T is the C diameter. While dwelling in C' under metal N, the electrons (holes) acquire a transversal momentum component $q = \pm((e/c) B_z y + t^2 g/v)$ where the former term is due to magnetic field whereas the last term is caused by the C/N tunneling coupling with energy $t^2 g$. Here t is the tunneling matrix element, g is the electron density of states in the metal stripe N, v is the Fermi velocity in C, and B_z is the magnetic induction directed along z -axis. For the rectangular geometry of Fig. 2a the trial wavefunction in C' under metal is constructed as

$$\Psi_{C'}(x, y) = (\alpha_x e^{ikx} + \beta_x e^{-ikx}) (\alpha_y u_n(\zeta_+) + \beta_y u_n(\zeta_-)) \quad (7)$$

where we have introduced auxiliary functions $u_n(\zeta) = \exp(-\zeta^2/2) H_n(\zeta)$, $H_n(\zeta)$ is the Hermite polynomial, $\zeta_{\pm} = \zeta(y, \pm k) = \sqrt{m\omega_{c0}/\hbar} (y \mp \beta^2 k) = q_0 y \mp \lambda_{c0} k$. Here $q_0 = \sqrt{m\omega_{c0}/\hbar}$, $\lambda_{c0} = (\omega_c/\omega_{c0})^2 \lambda^2 q_0$, $\lambda = \sqrt{\hbar/eB}$, $\omega_c = eB/m_e$ is the cyclotron frequency, m_e is the electron mass. The energy dependence of k then is $k(\varepsilon) = (\omega_{c0}/\omega_0)(\sqrt{2m\Delta_n/\hbar})\sqrt{(\varepsilon - \Delta_n)/\Delta_n}$ where $\Delta_n = E_s + \hbar\omega_{c0}(n + 1/2)$ and $\omega_{c0} = \sqrt{\omega_c^2 + \omega_0^2}$, ω_0 is the characteristic of steepness the confinement potential. In the above formulas we disregard the chirality effects [24] since the H/ C'' and C'/N transmissions are non-chiral. The trial wavefunctions in C and N outside the C/N-knot region are taken as mere plane waves. The boundary conditions (BC) yield the system of 8 non-linear transcendental equations for 8 coefficients entering the trial wavefunctions. The BC equations had been solved numerically which allows computing of the transmission probabilities $\mathcal{T}_y^{\text{left(right)}}$ and \mathcal{T}_x entering Eq. (1).

Using the above non-linear boundary conditions for the cross-stripe setup (Fig. 2a) to computing the transmission probabilities through the C/N-knot we have studied transport properties the C/N-knot. In Fig. 2a we show transmission coefficients for an electron incoming from C into the C' -section along the \hat{x} -direction, \mathcal{T}_x (dotted black curve), turning to the right, $\mathcal{T}_y^{\text{right}}$ (solid blue curve), and turning to the left, $\mathcal{T}_y^{\text{left}}$ (dashed red curve) obtained as solutions of the non-linear boundary conditions. Similar results had also been obtained for the nanotube-stripe (Fig. 1c) geometry. We show the numeric results in Fig. 2b where we also indicate parameters of the C/N-knot and the external magnetic field B_z . One can see that the transmission probabilities $\mathcal{T}_y^{\text{left(right)}}$ and \mathcal{T}_x are both experiencing strong resonances which suggest strong de-

flecting the electrons and holes from C to N in the lateral \hat{y} -direction at certain values the electron energy ε and magnetic field B_z . To emphasize the difference between the two NE mechanisms (i.e., phonon drag and thermal injection) we set either $\delta f^{\text{pd}} \equiv 0$ while $\delta f^{\text{th}} \neq 0$ or otherwise $\delta f^{\text{th}} \equiv 0$ while $\delta f^{\text{pd}} \neq 0$. In Fig. 2c we plot the non-equilibrium (NE) electron distribution function $f_C(\varepsilon)$ in the C section obtained as a self-consistent numeric solution of Eqs. (2), (3). Brown curve is $f_C(\varepsilon)$ altered only by the NE phonon drag whereas green curve is $f_C(\varepsilon)$ altered only by thermal injection the electron and holes at $\Gamma_{\text{HC}} = 0.3$. We have used the following parameters $\tau_{\text{ep}} = 10^{-12}$ s, $\sigma_0 = 0.2$, $N_0 = 1$, $\Delta_v = 1$, $T'_C = 0.1$ is the temperature in C'-section, $s = 0.02$ is the sound velocity, $v = 1$. In Fig. 2b and below, for the sake of convenience, the characteristics with energy and temperature dimensions are expressed in units the semiconducting gap Δ_v in C (we set $\hbar = 1$). Parameters with the wavenumber dimensions (like k , q_0 , q_c , etc.) are expressed in units Δ_v/v whereas the length parameters (like L , W , λ , λ_{c0} , etc.) are expressed in the units of v/Δ_v . Then, e.g., for a carbon nanotube (CNT) with diameter $d_T = 2.5$ nm one gets $\Delta_v = 2\hbar v/d_T = 0.4$ eV, $\Delta_v/v = 7.5 \times 10^8 \text{ m}^{-1}$ and $v/\Delta_v = 1.3$ nm where for CNT (and graphene) we also use that $v = 8.1 \times 10^5 \text{ m/s}$ and $s = 2.1 \times 10^4 \text{ m/s}$. Inset in Fig. 2c shows the phonon drag - induced NE deviation the distribution function $\delta f_{e,h}$ of electrons (blue curve) and holes (red curve) in the C section for the same parameters as listed above. Driving factor $\delta f_C = f_C - f_N = \delta f^{\text{pd}} + \delta f^{\text{th}}$ for the lateral magnetoelectric current I_{\perp} at $U_0 = 0$ is plotted in Fig. 2d. Red dashed curve corresponds to influence of the NE thermal injection only (we set for the moment $\delta f^{\text{pd}} \equiv 0$) while blue solid curve shows the combined influence of both, the NE thermal injection and the phonon drag.

In Fig. 3 we show transmission probabilities and MTEC versus magnetic field B_z and temperature deviation $\delta T^* = T^* - T_C$ where T_C is the steady state temperature of C. The effective electron temperature T^* which meters the NE effect is introduced as $T^* = \int_0^{\infty} d\varepsilon \cdot \varepsilon M_{\text{min}} \delta f_C$. In Fig. 3a we plot the longitudinal transmission probability through the C/N-knot versus the electron energy ε and the cyclotron wavenumber $q_c = \sqrt{eB_z/\hbar}$. The C/N-knot length and width are $L = 2.7$ and $W = 2.9$ respectively, $q_0 = 0.5$, $\lambda_0 = 5.5$, $U_0 = 0.5$. Computed lateral transmission probability is shown in Fig. 3b for the same C/N-knot parameters. In Fig. 3c we plot the lateral magneto-thermoelectric current (MTEC) I_{\perp} in units $\Delta(e/h)$ induced along N versus the cyclotron wavenumber q_c (in units Δ/v) for different effective temperature deviations $\delta T^* = 0.08, 0.8, 1.4$, and 2 in units Δ for curves 1-4 respectively) along the \hat{x} -axis in C. As an illustration, we also show the corresponding contour plot of MTEC for the same C/N-knot parameters. Maximums the heat-generated electric cur-

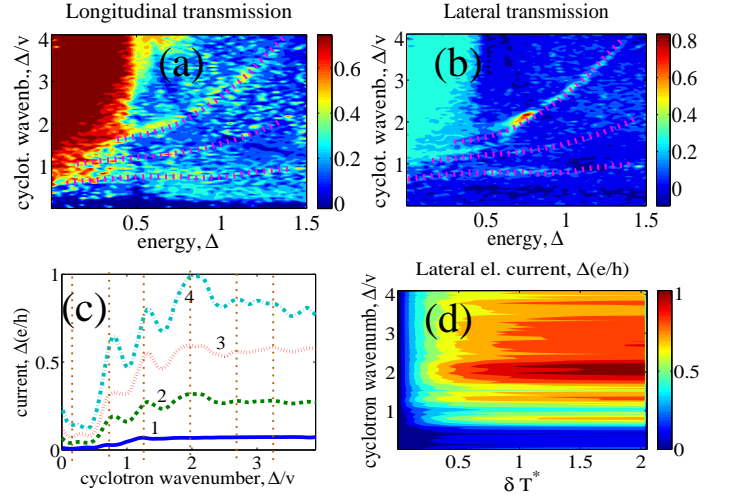


FIG. 3: Color online. (a) Longitudinal transmission probability through the C/N-knot versus the electron energy and the cyclotron wavenumber $q_c = \sqrt{eB_z/\hbar}$ (see parameters in text). (b) Lateral transmission probability computed for the same C/N-knot parameters. (c) Lateral magneto-thermoelectric current (MTEC) I_{\perp} induced along N versus the cyclotron wavenumber q_c for different temperature deviations δT^* (see text) in C. (d) Corresponding contour plot of steady state MTEC for the same C/N-knot parameters.

rent in N correspond to geometrical resonances when different Landau orbits match the C/N-knot dimensions. From Fig. 3d one can also see that I_{\perp} is roughly proportional to the temperature deviation δT^* in C. The magnetic field induction B_z and the temperature deviation δT^* both facilitate increasing the electric current I_{\perp} (see, i.e., Figs. 3c,d) at the expense of non-equilibrium phonon drag and thermal injection.

The obtained results suggest that after penetrating from C' to N under influence the Lorentz force (see Fig. 1b), the electrons (e) and holes (h) propagate inside N in opposite directions. Since the electrons and holes also have opposite electric charges, they create a substantial electric current $I_e = I_h = I \neq 0$ flowing along N. Magnitude the thermally induced electric current in N is proportional to the heat flow in C and it also depends on the d.c. magnetic field \mathbf{B} . A finite field $\mathbf{B} \neq 0$ splits the heat flow and separates the electrons and holes from each other as is shown in Fig. 1a.

The consideration above neglects the role of electron-electron and electron-hole interaction in thermal transport. However many-body effects might be essential in a system where the NE electron density $n^* = \int_0^{\infty} d\varepsilon \cdot M_{\text{min}} \delta f_C$ is high. One application of the suggested here heat stream splitting is to probing the electron-electron interaction and determining the exciton binding energy E_g . For low temperatures and small δT^* when $E_g > T_C$, the excitons transfer the heat from C'' to C'. Since the excitons have no electric charge, there is no splitting of

heat flow in the C/N-knot, and no lateral electric current ($I_{\perp} \equiv 0$) is induced in N. However I_{\perp} turns being finite as soon as the local temperature $T'_C \leq T^*$ in the C/N-knot vicinity exceeds the threshold value T_C^{thr} which corresponds to the binding energy E_g , i.e., $T_C^{\text{thr}} \simeq E_g < T'_C \leq T^*$ and no excitons are formed in C any more. Thus presence of the threshold temperature T_C^{thr} which turns I_{\perp} on indicates creating of excitons inside C with the binding energy $E_g \simeq T_C^{\text{thr}}$. The considered here approach might provide an efficient thermoelectric solution which exploits splitting the thermal current components by so-called C/N-knot. Suggested generation of electric current potentially can be used in thermoelectric energy generators and coolers. [3–6]

I wish to thank P. Kim and V. Chandrasekhar for fruitful discussions. This work had been supported by the AFOSR grant FA9550-11-1-0311.

-
- [1] C. L. Kane and E. J. Mele, Phys. Rev. Lett. **95**, 146802 (2005).
 - [2] C. L. Kane and M. P. A. Fisher, Phys. Rev. B, **55**, 15832 (1997).
 - [3] D. M. Rowe (Editor), *Thermoelectric Handbook*, (Chemical Rubber Company, Boca Raton, Fla., 1995).
 - [4] J. P. Small, K. M. Perez, and P. Kim, Phys. Rev. Lett., **91** 256801 (2003).
 - [5] Y.-M. Lin, X. Sun, and M. S. Dresselhaus, Phys. Rev. B, **62** 4610 (2000).
 - [6] S. E. Shafranjuk, EPL **87**, 57007 (2009).
 - [7] S. E. Shafranjuk, in Nanosensors of External Fields (Ed. Nalwa) 413-454 (Encyclopedia of Nanoscience and Nanotechnology, American Scientific Publishers, **8** 2011).
 - [8] E. Pop, D. A. Mann, K. E. Goodson, and H. Dai, J. Appl. Phys. **101**, 093710 (2007).
 - [9] A. I. Persson, Y. Kan Koh, D. G. Cahill, L. Samuelson, and H. Linke, Nano Lett., **9**, 4484 (2009).
 - [10] M. Bailyn, Phys. Rev. **157** 480 (1967).
 - [11] U. Bockelmann and G. Bastard, Phys. Rev. B **42**, 8947 (1990).
 - [12] S. E. Shafranjuk, arXiv:1208.4112 [cond-mat.mes-hall].
 - [13] S. Datta, *Electronic Transport in Mesoscopic Systems* (Cambridge Univ. Press, Cambridge, 1997).
 - [14] M. C. Lemme, T. J. Echtermeyer, M. Baus, and H. Kurz, IEEE Electron Device Lett. **28**, 282 (2007).
 - [15] H. Xu, S. Wang, Z. Zhang, Z. Wang, H. Xu, and L.-M. Peng, Appl. Phys. Lett., **100**, 103501 (2012).
 - [16] F. Xia, V. Perebeinos, Y.-m. Lin, Y. Wu, and Ph. Avouris, Nature Nanotechnology, **6**, 179 (2011).
 - [17] A. F. Young, and P. Kim, Nature Phys., **5**, 222 (2009).
 - [18] M. A. N. Araujo, and P. D. Sacramento, Phys. Rev. B **77**, 134519 (2008).
 - [19] F. Rana, Phys. Rev. B **76**, 155431 (2007).
 - [20] L. V. Keldysh, [Zh. Eksp. Teor. Fiz. 47, 1515 (1964)] Sov. Phys. JETP **20**, 1018 (1965).
 - [21] T. D. Musho and D. G. Walker, J. Mater. Res., **26**, 1993 (2011).
 - [22] T. Yamamoto and K. Watanabe, Phys. Rev. Lett. **96**, 255503 (2006).
 - [23] L. G. C. Rego and G. Kirczenow, Phys. Rev. Lett. **81**, 232 (1998).
 - [24] T. Ando, J. Phys. Soc. Jpn **74**, 777 (2005).
 - [25] M. Tsousidou and K. Papagelis, in Physics of Semiconductors, 28th International edited by W. Jantsch and F. Schäffler (2007) 1045.